J Solid State Electrochem (2012) 16:443–448
DOI 10.1007/s10008-011-1351-6

ORIGINAL PAPER

Preparation and performance of porous titania with a trimodal pore system as anode of lithium ion battery

Jin Yi · Dongsheng Lu · Xiaoping Li · Shejun Hu · Weishan Li · Jianfei Lei · Yuan Wang

Received: 13 December 2010 / Revised: 4 February 2011 / Accepted: 18 February 2011 / Published online: 6 April 2011

Abstract A porous titania has been prepared by using polystyrene spheres and tri-block copolymer ($(EO)_{20}$–$(PO)_{70}$–$(EO)_{20}$, P123) as templates, and its structure, composition, and performance as anode of lithium ion battery are characterized by scanning electron microscopy (SEM), transmission electron microscopy (TEM), X-ray diffraction, and galvanostatic charge/discharge test. The results from SEM and TEM indicate that the prepared porous titania has a trimodal pore system, in which the pores are in ordered arrangement and interconnected with the same pore diameter and uniform wall thickness. The charge/discharge tests show that the battery using the prepared porous titania as anode exhibits good rate capacity and cycle stability.

Keywords Porous titania · Lithium ion battery · Rate capacity · Cycle stability

J. Yi · D. Lu · X. Li · S. Hu · W. Li · J. Lei · Y. Wang
School of Chemistry and Environment,
South China Normal University,
Guangzhou, China

X. Li · W. Li
Key Laboratory of Electrochemical Technology
on Energy Storage and Power Generation
of Guangdong Higher Education Institutes,
Guangzhou, China

X. Li · W. Li (✉)
Engineering Research Center of Materials and Technology
for Electrochemical Energy Storage, Ministry of Education,
Guangzhou, China
e-mail: liwsh@scnu.edu.cn

Introduction

Owing to its largest energy density among all the commercial secondary batteries, lithium ion battery is believed to be a good power source for electric vehicles and an efficient energy storage device for solar energy exploitation [1–5]. However, the safety and cycle life of the present commercial lithium ion battery cannot meet the requirement of its applications in these areas due to the use of graphite as anode. Titania has high safety and long cycle life and is a promising alternative to graphite as anode of lithium ion battery, but its rate capacity needs to be improved. Therefore, many efforts are focused on the development of new titania materials that have fast kinetics for lithium ion insertion/de-insertion, such as nanotubes [6], mesoporous microspheres [7], and hollow microspheres [8]. Among these materials, porous titania is effective for the improvement in kinetics of lithium ion insertion/de-insertion since the pore structure provides the materials with more ion transportation paths and a large surface area for charge transfer reaction [9–11].

Tri-block copolymer (EO–PO–EO; EO, ethylene oxide; PO, propylene oxide) has been widely used as a structure-directing agent in a cooperative assembly process to prepare mesoporous and microporous materials with inorganic frameworks [12]. It has also been found that the pore structure of inorganic materials can be improved by using dual templates, such as using polystyrene (PS) and tri-block copolymers as templates simultaneously [13]. In this paper, PS spheres and $(EO)_{20}$–$(PO)_{70}$–$(EO)_{20}$ (P123) were used as dual templates for the preparation of porous titania with a trimodal pore system, with the aim to improve the rate capacity of titania as anode of lithium ion battery.

Experimental

Preparation of materials

Noncross-linked, monodisperse polystyrene spheres were synthesized by using emulsifier-free polymerization techniques as described in literature [14]. Styrene (Sinopharm Chemical Reagent Co., Ltd.) was washed first with 0.1 M NaOH three times and then with deionized water three times. The washed styrene (26 mL) and 1.25 wt.% sodium persulfate solution (40 mL) were added successively into a mixture of 200 mL deionized water and 1.8 g polyvinylpyrrolidone at 70 °C under stirring in N_2 atmosphere. The reaction proceeded at 70 °C for 24 h, and PS spheres were obtained by centrifugalizing the resulting mixture.

The precursor of titania was prepared by mixing absolute ethanol, acetic acid, hydrochloric acid, deionized water, tetrabutyltitanate, and P123 in the molar ratio: $Ti(obu)_4$: EtOH: HAC: HCl: H_2O: P123=1: 10: 0.6: 7: 2: 0.05, under stirring for 30 min. Then, 4 g of polystyrene spheres was added for mixing under stirring for another 12 h at room temperature. Finally, the polystyrene spheres were separated from the mixture by centrifugation and dried under vacuum at 60 °C for 4 h. The dried PSs containing the titania precursor were calcined in air atmosphere at 250, 350, and 500 °C successively, each for 2 h, and finally, the porous titania sample was obtained.

Structure and morphology characterization

The crystal structure of the prepared sample was characterized by X-ray diffraction (XRD) (Rigaku D/MAX-RC, Japan) with CuKα radiation (wavelength=1.54178 Å) at 36.0 kV and 20 mA. The scattering angle range used in the measurements was from 20° to 80°. Fourier transform infrared (FT-IR) spectra were obtained with a PerkinElmer instrument (USA) using the KBr pellet technique. The morphology of the sample was observed with scanning electron microscopy (SEM) (JEOL, JSM-6380LV, JSM-6330F, Japan) and transmission electron microscopy (TEM) (JEOL, JEM-2010HR, Japan). The N_2-sorption isotherm curve was recorded at 77 K on Micromeritics ASAP 2020 instrument (USA). The specific surface area was calculated by the Brunauer–Emmett–Teller (BET) method; pore sizes and volumes were estimated from pore size distribution that was obtained from the desorption branch of the isotherm curve. Thermal analysis (TG-DSC) was carried out by using a NETZSCH STA 409C thermal analyzer (Germany).

Electrochemical measurements

Working electrodes were prepared as follows: 80 wt.% porous titania sample as active material, 10 wt.% acetylene black as conducting agent, and 10 wt.% polyvinylidene fluoride as binder were mixed in *N*-methylpyrrolidone. The working electrodes were obtained by coating the mixture on copper foils with doctor-blade technique and drying in air at 85 °C for 2 h and then in a vacuum oven at 120 °C for 4 h.

Electrochemical measurements were carried out by using coin-type test cells, where Li metal foil was used as the counter electrode. The electrolyte was 1 M $LiPF_6$ dissolved in a mixture of ethylene carbonate, dimethyl carbonate, and diethyl carbonate (1:1:1 by volume). The separator of cell was Celgard 2400. CR2032-type coin cells were assembled in an Ar-filled glove box (Mikrouna, Super 1220/750/900). The assembled cells were aged overnight before testing. Galvanostatic charge/discharge tests were performed by using a LAND cell test (Land CT 2001A) system, at different current densities in the voltage range of 1–2.5 V vs. Li^+/Li. For comparison, the cell with commercial titania (P25, Germany) as working electrode was also set up and tested under the same conditions. The unit weights of active materials in the composite working electrodes were about 3.2±0.2 mg cm^{-2}, and the surface and thickness of the working electrodes were 1 cm^2 and 40 μm, respectively.

Results and discussion

The X-ray diffraction pattern of the prepared titania is shown in Fig. 1. The diffraction peaks of prepared titania are in good agreement with the standard card (JCPDS; card no., 21-1272), indicating that the prepared sample has a pure crystal structure of anatase.

The SEM image in Fig. 2 shows that the as-prepared PSs have a diameter of about 200 nm. The SEM and TEM images of the prepared porous TiO_2 are shown in Fig. 3. It can be seen that the prepared sample has an ordered and interconnected pore structure with the same pore diameter

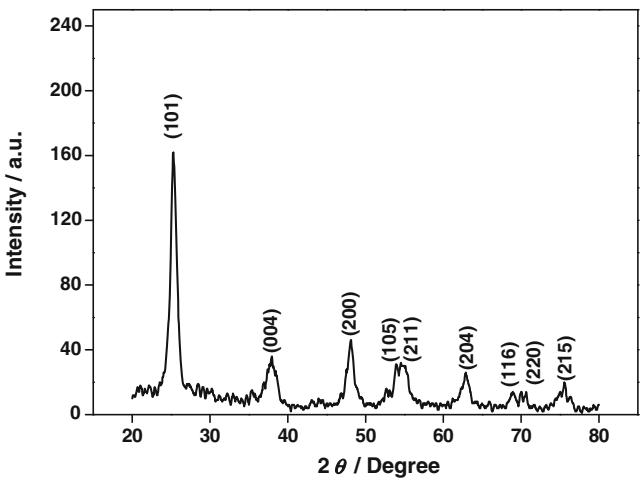

Fig. 1 XRD pattern of the prepared porous titania

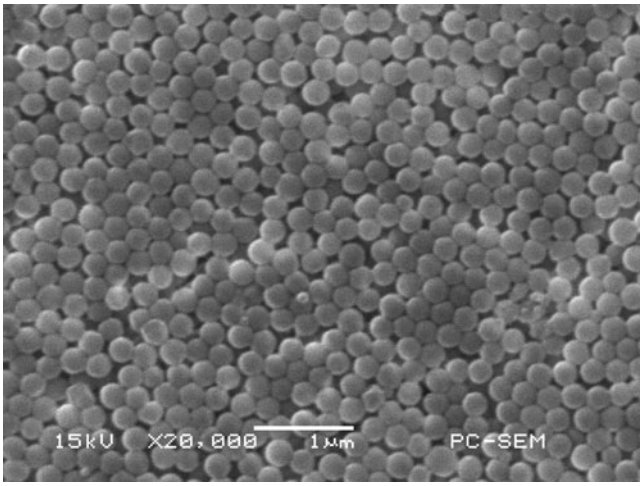

Fig. 2 SEM image of PS spheres used as templates

and uniform wall thickness through the formation of the close-packed arrangement of PSs by centrifugation. The size of the pores formed from the PSs is about 160 nm, which is slightly smaller than that of the PSs due to shrinkage during calcinations. The thickness of the wall formed between two holes is about 25 nm, and the pore sizes of the small holes that connects neighboring big holes (160 nm) are about 30–40 nm. It can be seen from the TEM image (Fig. 2b) that the wall of the porous titania consists of titania nanoparticles with an average diameter of 10 nm.

In order to understand the formation process of the porous titania, infrared spectroscopy measurements were carried out. The FT-IR spectrum of the precursor is shown in Fig. 4a. The absorption peak at 3,379 cm^{-1} is due to the stretching vibration of O–H in the titanium sol. Four characteristic peaks from 1,600 to 1,450 cm^{-1} are ascribed to the phenyl ring of the PS. The C–H stretching and bending vibrations in the phenyl ring contribute to the sharp peaks at 3,021 cm^{-1} and 697 cm^{-1}. The peak around 1,470 cm^{-1} can be ascribed to the $–CH_2–$ bending vibration. These peaks are characteristic of PS [15]. The sharp peaks at 2,917 cm^{-1}, 1,075~1,020 cm^{-1}, and 1,275~1,200 cm^{-1} are corresponding to the C–H stretching vibration, symmetric and asymmetric stretching vibrations of C–O in P123, respectively. The peak at about 1,109 cm^{-1} is derived from the Ti–O–C stretching vibration. It is obvious that PS, P123, and tetrabutyltitanate exist in the precursor.

The FT-IR spectrum of porous titania is shown in Fig. 4b, which is almost consistent with that of the standard TiO_2 [16]. The typical peaks of PS and P123 disappear, indicating that PS and P123 have been converted completely after calcination. The peaks at 3,417 cm^{-1} and 1,633 cm^{-1} are corresponding to the surface-adsorbed H_2O and –OH of TiO_2 [17, 18]. The wide peak around 667 cm^{-1} is ascribed to the vibration of the Ti–O bond in TiO_2 [17]. The peak at 1,128 cm^{-1} is corresponding to the Ti–O–C stretching vibration. This suggests that the small amount of carbon from the conversion of PS and P123 remains in titania [9, 19].

The conversion of the precursor into TiO_2 can be confirmed from the weight losses of the precursor upon calcination, as shown in Fig. 5. The total weight loss before 500 °C is 84.5%. Two obvious weight losses of different extents in the temperature range of 29–500 °C can be observed. The first weight loss at 29–350 °C is mainly due to the desorption of physisorbed water and the burning of P123 and organic substances (such as HAC, EtOH) in the precursor, which are corresponding to the endothermic peak at 80 °C and the exothermic peak at 350 °C in the DSC curve [20]. The second weight loss at 350–500 °C can be attributed to the decomposition of PS and the transformation of titanate into anatase, which is accompanied by the

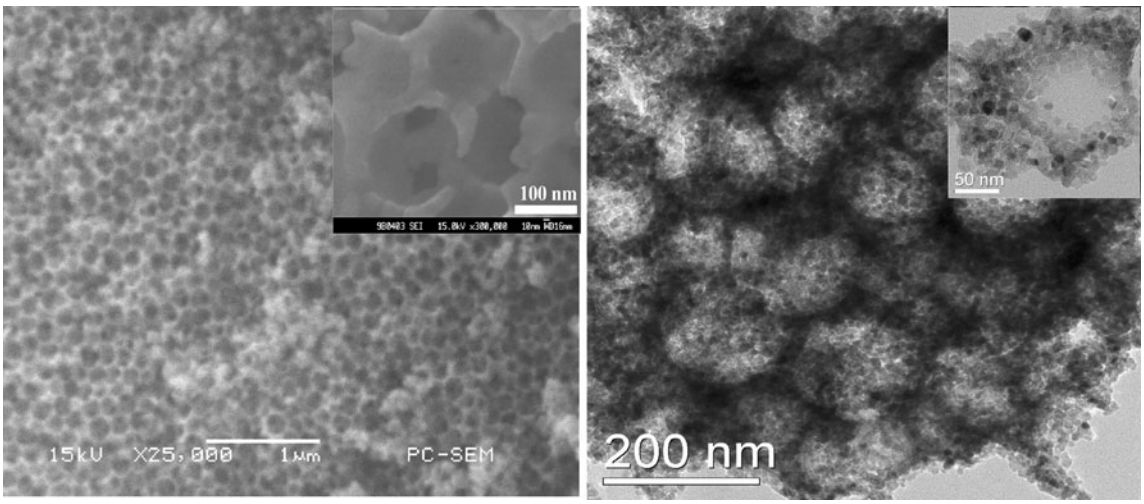

Fig. 3 SEM (**a**) and TEM (**b**) images of the porous TiO_2. The *insets* are the high magnification images

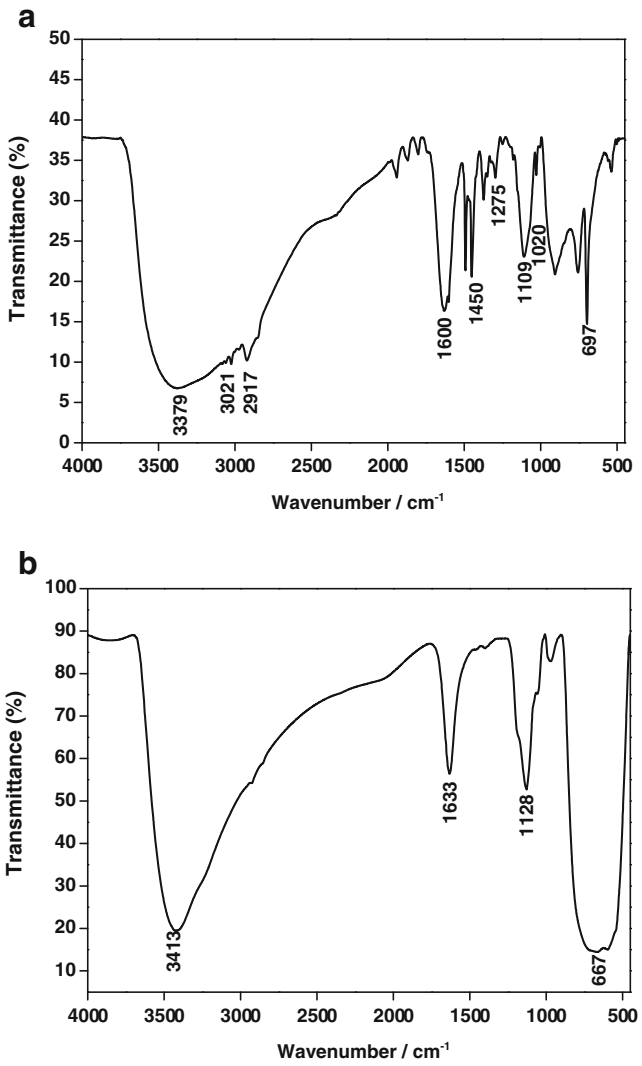

Fig. 4 FT-IR spectra of the precursor (**a**) and the porous titania (**b**)

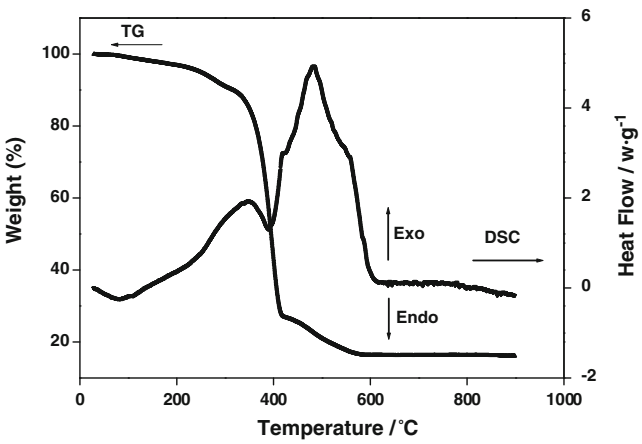

Fig. 5 TG-DSC profiles of the precursor

large endothermic peak of at 400 °C and the exothermic peak at 480 °C in the DSC curve [21, 22]. From 500 to 900 °C, no more weight loss occurs, indicating that the preparation of porous titania can be completed before 600 °C. In addition, it is obvious that both templates have been converted completely during the calcination, which is in agreement with the result of the FT-IR spectrum shown in Fig. 4b.

Figure 6 presents the adsorption/desorption isotherm curves of the porous titania along with its pore size distribution derived from the desorption branch of the isotherm curve. The type-IV with type H1 hysteresis loop isotherm of the prepared sample is characteristic of macroporous solid materials, which is similar to the porous titania in the literature [23]. It can be seen that the adsorption/desorption curve is reversible, indicating a highly uniform pore size without obvious pore-blocking effect. Meanwhile, the existence of slightly blocked mesopores with larger pore size is indicated by a moderately steep condensation step and a small hysteresis loop on the isotherm at the high relative pressure P/Po≈0.85 [24]. From the Barrett–Joyner–Halenda (BJH) curve, it can be seen that the macroporous titania contains two distinguishable types of pores with different sizes between 2 and 50 nm. The mesopores of 30 nm can be ascribed to the small holes (30–40 nm) that connect neighboring big holes, as shown in Fig. 3a, while the mesopores of 4 nm are generated by the micelle formation of the EO–PO–EO tri-block copolymer, where a solid impenetrable core is generated by the hydrophobic PO, and the hydrophilic EO tails project more loosely around this core [14]. Thus, the formation of the mesopores may be attributable to P123 through a cooperative assembly process. From the above discussion, it can be concluded that the prepared porous titania has a trimodal pore system [24, 25], with macropore (about 160 nm) and dual

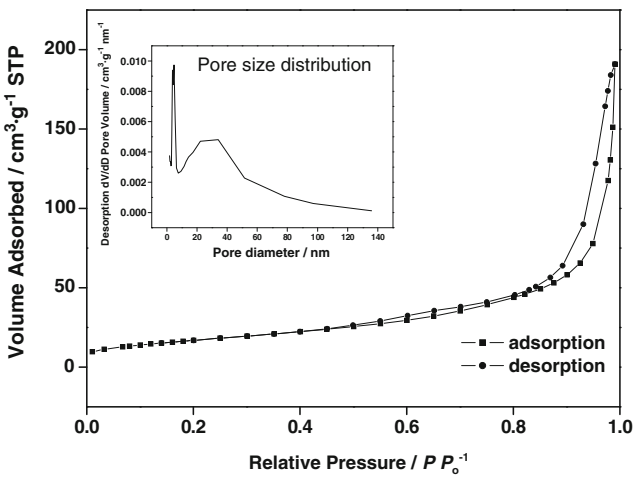

Fig. 6 Nitrogen adsorption/desorption isotherm curves and BJH pore size distribution (*inset*) of the porous titania

mesopore (about 4 and 30 nm). The overall BET surface of the porous titania is 58.85 m^2 g^{-1}, which is much larger than that of mesoporous titania prepared by PS as template [9] and commercial sample P25 (about 50 m^2 g^{-1}).

The charge/discharge profiles of the prepared porous titania and commercial P25 at a current density of 8.4 mA g^{-1} are shown in Fig. 7. It can be seen that, in the first cycle, the discharge and charge capacities are 286 and 218.2 mAh g^{-1} for the porous titania, while 225.8 and 143.9 mAh g^{-1} for commercial P25, respectively. Another feature of interest is that the first discharge curve can be divided into three domains. The first domain (voltage decreasing from 2.5 to 1.75 V) characterized by a monotonous potential decrease corresponds to a solid solution insertion mechanism [15]. The second domain (voltage at about 1.75 V) indicates the phase equilibrium between anatase TiO_2 and anatase $Li_{0.5}TiO_2$, within which half of Ti^{4+} is converted to Ti^{3+} along with the insertion of Li ions. In the third stage, another voltage decrease from 1.75 to 1.0 V (vs. Li^+/Li) appears, which can be ascribed to the insertion of lithium ions into the surface layers of TiO_2 after all the available interstitial octahedral sites inside the anatase crystals are filled. The larger capacity of the prepared porous titania than P25 confirms that the third stage of Li insertion is mainly a surface effect as well [26].

Figure 8 presents the rate and cycle performance of the prepared porous titania in comparison with the commercial P25. The specific current used for the electrodes was from 8.4 to 336 mA g^{-1}. When a specific current of 8.4 mA g^{-1} is applied to the porous titania electrode, a specific charge capacity of 210.9 mAh g^{-1} is obtained, which is higher than that of mesoporous titania synthesized without P123 [9]. The average specific capacities are 183, 168, and 135 mAh g^{-1} for the specific currents of 16.8, 168, and 336 mA g^{-1}, respectively, which are comparative to those porous TiO_2 samples that have been reported [7, 11, 26]. For example, the reversible capacity is 156 mAh g^{-1} for mesoporous microspheres at 204 mA g^{-1} [7], 145 mAh g^{-1}

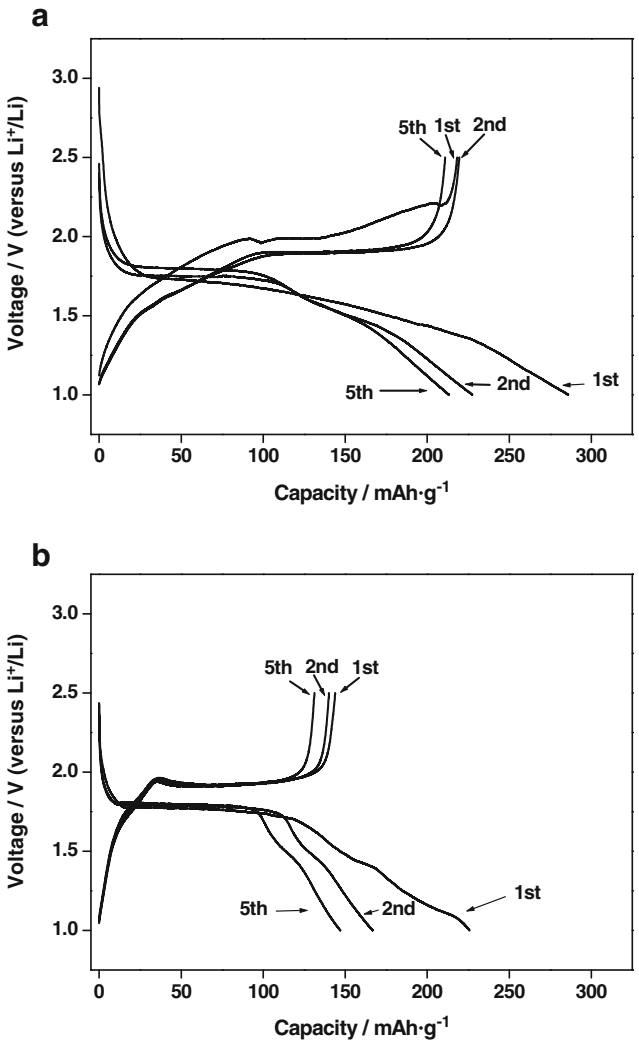

Fig. 7 Charge/discharge profiles of the porous titania (**a**) and commercial P25 (**b**) at a current density of 8.4 mA g^{-1}

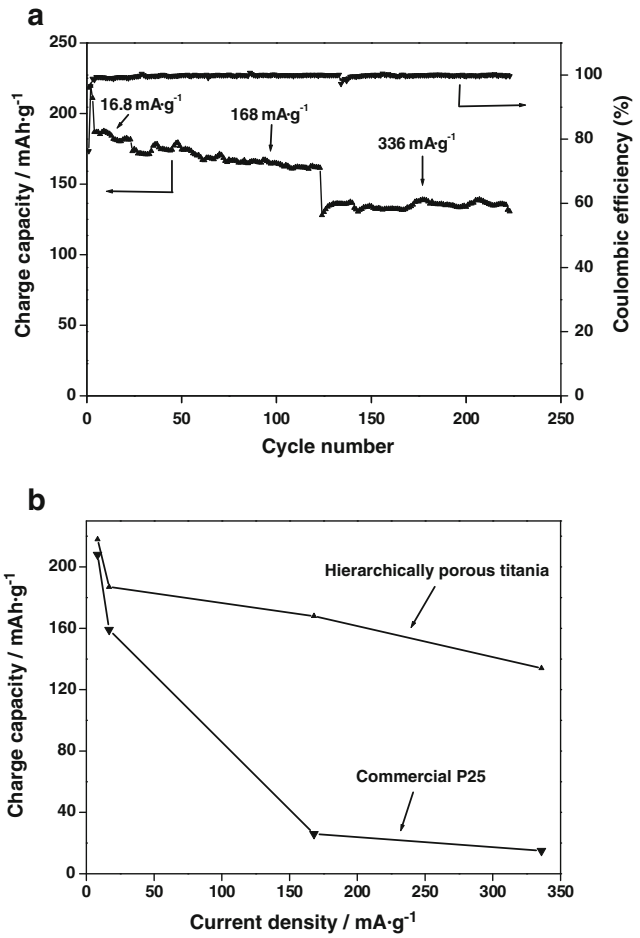

Fig. 8 Cyclic performance of porous titania at different charge/discharge current densities (**a**) and the dependence of discharge capacity on the charge/discharge rates compared with the commercial P25 (**b**)

for porous TiO_2 nanowire at 168 mA g^{-1} [11], and about 150 mAh g^{-1} for porous anatase TiO_2 at 120 mA g^{-1} [26].

It can be noted that the capacity loss of the porous titania can be neglected when cycling at different rates; for example, the capacity is 187 mAh g^{-1} for the first cycle and remains 181.6 mAh g^{-1} after 20 cycles at 16.8 mA g^{-1}. This indicates that the porous titania also has better cyclic performance. Compared with the commercial P25, the porous titania exhibits a better rate performance, as shown in Fig. 8b. Apparently, the better performance of the prepared porous titania results from its special pore structure.

Conclusions

A new method for the preparation of porous titania with a novel pore system has been reported in this paper. With PS spheres and tri-block copolymer (P123) as dual templates, the prepared porous titania which has a trimodal pore system can be obtained. This pore system provides TiO_2 with fast kinetics of lithium ion insertion/de-insertion for its application as anode of lithium ion battery, and thus, the TiO_2 exhibits a high rate capacity and good cycle stability which can meet the demand of lithium ion battery for application in electrical vehicles.

Acknowledgments The authors gratefully acknowledge financial support from the National Natural Science Foundation of China (grant no. NSFC20873046), Specialized Research Fund for the Doctoral Program of Higher Education (grant no. 200805740004), and Natural Science Foundation of Guangdong Province (grant no. 10351063101000001).

References

1. Rao MM, Liu JS, Li WS, Liao YH, Liang Y, Zhao LZ (2010) J Solid State Electrochem 14:255
2. Liu HJ, Wang XM, Cui WJ, Dou YQ, Zhao DY, Xia YY (2010) J Mater Chem 20:4223
3. Zhang CF, Quince M, Chen ZX, Guo ZP, Liu HK (2010) J Solid State Electrochem. doi:10.1007/s10008-010-1256-9
4. Adams S (2010) J Solid State Electrochem 14:1787
5. Koudriachova MV (2010) J Solid State Electrochem 14:549
6. Wei Z, Liu Z, Jiang RR, Bian CQ, Huang T, Yu AS (2010) J Solid State Electrochem 14:1045
7. Wang J, Zhou YK, Hu YY, O'Hayre R, Shao ZP (2010) J Phys Chem C. doi:org/10.1021/jp1087509
8. Song B, Liu SW, Jian JK, Lei M, Wang XJ, Li H, Yu JG, Chen XL (2008) J Power Sources 180:869
9. Fu LJ, Zhang T, Cao Q, Zhang HP, Wu YP (2007) Electrochem Commun 9:2140
10. Wang KX, Wei MD, Morris MA, Zhou HS, Holmes JD (2007) Adv Mater 19:3016
11. Shim HW, Lee DK, Cho IS, Hong KS, Kim DW (2010) Nanotechnology 21:255706
12. Holland BT, Blanford CF, Do T, Stein A (1999) Chem Mater 11:795
13. Yang PD, Deng T, Zhao DY, Feng PY, Pine D, Chmelka BF, Whitesides GM, Stucky GD (1998) Science 282:2244
14. Sen T, Tiddy GJT, Casci JL, Anderson MW (2003) Angew Chem Int Ed 42:4649
15. Sudant G, Baudrin E, Larcher D, Tarascon JM (2005) J Mater Chem 15:1263
16. Venkatachalam N, Palanichamy M, Murugesan V (2007) J Mol Catal A: Chem 273:177
17. Tong TZ, Zhang JL, Tian BZ, Chen F, He DN (2008) Mater Lett 62:2970
18. Naik B, Parida KM, Gopinath CS (2010) J Phys Chem C 114:19473
19. Liu GQ, Jin ZG, Liu XX, Wang T, Liu ZF (2007) J Sol Gel Sci Technol 41:49
20. Sung CC, Fung KZ, Hung IM, Hon MH (2008) Solid State Ionics 179:1300
21. Lukens WW, Stucky GD (2002) Chem Mater 14:1665
22. Strohm H, Lobmann P (2004) J Mater Chem 14:2667
23. Carbajo MC, Enciso E, Torralvo MJ (2007) Colloids Surf A Physicochem Eng Asp 293:72
24. Yang G, Hu P, Cao YB, Yuan FL, Xu RF (2010) Nanoscale Res Lett 5:1437
25. Lemaire A, Su BL (2010) Langmuir 26:17603
26. Bao SJ, Bao QL, Li CM, Dong ZL (2007) Electrochem Commun 9:1233